Table 1 Crystallographic parameters and model refinement statistics

	Wild-type	Wild-type	Wild-type	C353A	H351A	H351A	H351A
PDB code	3WQC	3WQD	3WQF	3WQG	4PB3	4PB4	4PB5
Bound metal	Mg	Mg	–	–	Mg	Mg	Mg
Substrate/inhibitor	–	D-EHA	–	–	–	2-amino maleic acid	L-EHA
Data collection							
Beam line	BL-17A	NE-3A	BL-17A	BL-17A	NW-12A	NW-12A	NW-12A
Wavelength (Å)	0.98000	1.00000	0.98000	0.98000	1.00000	1.00000	1.00000
Resolution (Å)	50–1.50 (1.53–1.50)[a]	50–1.50 (1.53–1.50)[a]	50–2.30 (2.34–2.30)[a]	50–1.55 (1.58–1.55)[a]	50–1.70 (1.73–1.70)[a]	50–1.80 (1.83–1.80)[a]	50–1.90 (1.93–1.90)[a]
Space group	$I4_122$	$I4_122$	$I4_122$	$I4_122$	$I4_122$	$I4_122$	$I4_122$
Cell parameters (Å)	$a=b=157.7$, $c=158.8$	$a=b=157.8$, $c=158.2$	$a=b=157.8$, $c=157.9$	$a=b=158.0$, $c=159.1$	$a=b=157.6$, $c=158.2$	$a=b=157.7$, $c=157.4$	$a=b=157.6$, $c=157.5$
Unique reflections	157,557	156,137	44,400	144,006	107,707	91,233	77,555
R_{merge}[b]	0.089 (0.765)	0.082 (0.591)	0.112 (0.727)	0.094 (0.857)	0.059 (0.464)	0.094 (0.672)	0.087 (0.585)
Completeness (%)	100.0 (100.0)	99.6 (100.0)	100.0 (100.0)	99.8 (100.0)	100.0 (100.0)	99.6 (99.1)	100.0 (100.0)
Redundancy	14.7 (14.6)	14.5 (13.5)	14.7 (14.7)	14.6 (14.5)	14.1 (8.5)	14.9 (15.0)	14.8 (14.8)
I/σ (I)	33.6 (5.0)	37.1 (6.5)	28.6 (7.1)	29.0 (5.6)	38.3 (5.4)	29.1 (5.4)	32.1 (7.0)
Refinement							
R_{work}/R_{free}[c,d]	0.121/0.152	0.144/0.176	0.198/0.239	0.143/0.179	0.166/0.185	0.164/0.183	0.153/0.187
RMSD bond length (Å)	0.026	0.026	0.018	0.025	0.026	0.025	0.025
RMSD bond angle (°)	2.18	2.10	1.90	2.14	2.3	2.2	2.1
Average B factor (Å^2)							
Overall	21.6	24.2	40.6	23.5	22.9	21.6	22.0
Protein	20.4	23.1	40.7	22.7	22.4	21.4	21.6
PLP	15.5	17.4	34.1	17.5	16.2	16.0	16.4
Metal (active-site Mg)	14.4	18.7	–	–	13.0	25.5	30.5
Substrate/inhibitor	–	19.0	–	–	–	27.9	26.3
Waters	32.2	34.1	38.6	31.6	28.2	24.5	26.7
Ramachandran plot (%)							
Favored	92.0	92.3	91.1	91.5	91.5	92.1	91.1
Allowed	7.4	7.4	8.4	7.9	8.2	7.6	8.6
Disallowed[e]	0.6	0.3	0.5	0.6	0.3	0.3	0.3

[a] Values in parentheses refer to data in the highest resolution shell

[b] $R_{merge}=\Sigma_h \Sigma_i|I_{h,i}-\langle I_h\rangle|/\Sigma_h\Sigma_i I_{h,i}$, where $\langle I_h\rangle$ is the mean intensity of a set of equivalent reflections

[c] $R_{work}=\Sigma\,|F_{obs}-F_{calc}|/\Sigma\,F_{obs}$ for 95 % of the reflection data used in the refinement. F_{obs} and F_{calc} are observed and calculated structure factor amplitudes, respectively

[d] R_{free} is the equivalent of R_{work}, except that it was calculated for a randomly chosen 5 % test set excluded from refinement

[e] The residues found in the disallowed regions of the Ramachandran plot are Arg141, Phe241, and Ser284; all of these residues have well-defined electron density and their main-chain conformations are reliable

NADH at 340 nm using a DU800 spectrophotometer (Beckman Coulter, Inc., Brea, CA). Assay was performed using a coupling system with NADH-dependent malate dehydrogenase (MDH), as described previously (Wada et al. 1999). The standard assay mixture consisted of 100 mM Tris-HCl buffer (pH 8.0), 0.01 mM PLP, 0.1 mM $MnCl_2$, 10 mM D-THA or L-EHA as a substrate, 0.32 mM NADH, ten units of MDH, and an appropriate amount of the enzyme in a total volume of 0.5 mL. The reactions were carried out at 30 °C with addition of the substrate. Reaction mixtures without substrate served as controls. One unit of the enzyme is defined as 1 μmol of NADH utilized per minute at 30 °C on the basis of an absorption coefficient of 6.22 mM^{-1} cm^{-1} at 340 nm.

Chemical synthesis of DL-*erythro*-3-hydroxyaspartate

DL-*erythro*-3-Hydroxyaspartate (DL-EHA) was synthesized by ammonolysis of a (±)-*trans*-epoxysuccinic acid at 60 °C. Reaction product was evaporated to dryness, and the resulting residue was dissolved in an acidified water (pH 2.0 adjusted with HCl). Water solution was allowed to stand for 16 h at 4 °C. The appeared crystals of 3-hydroxyaspartate were collected by filtration, washed with a small amount of the acidified water, and subsequently dried in vacuum for 24 h. Resulting product was confirmed by thin-layer chromatography (TLC) and high-performance liquid chromatography (HPLC) as described in the analytical methods.

Enzymatic optical resolution of DL-racemic 3-hydroxyaspartate

Purified D-THA DH was used to prepare L-THA or D-EHA from the corresponding racemates by an enzymatic optical resolution. The reaction mixture consisted of 100 mM Tris-HCl buffer (pH 8.0), 0.01 mM PLP, 0.1 mM $MnCl_2$, 200 mM DL-THA or DL-EHA, and purified D-THA DH in a total volume of 100 mL. Reactions were performed at 30 °C with reciprocal shaking at a speed of 90 rpm and started by addition of 0.66 mg of the enzyme to DL-THA solution and 0.87 mg to DL-EHA solution. Incubation was continued for 9 or 12 h, respectively. During incubation, D-form and L-form of 3-hydroxyaspartate in the reaction mixture were monitored using HPLC and an amino acid analyzer as described below. Samples taken for the analyses were heated at 70 °C for 30 min to inactivate the enzyme. After incubation, L-THA or D-EHA in the reaction product was isolated by crystallization as described below.

Isolation of L-*threo*-3-hydroxyaspartate or D-*erythro*-3-hydroxyaspartate

The reaction product was acidified to pH 2.0 using HCl. Resulting solution was evaporated to about 10 mL and subsequently allowed to stand for 16 h at 4 °C. Appeared crystals of 3-hydroxyaspartate were collected with the same procedure as for the preparation of DL-EHA. TLC, HPLC, and nuclear magnetic resonance (NMR) spectroscopy, as described in the analytical methods, confirmed the resulting product.

Analytical methods

Thin-layer chromatography Crystallized DL-EHA, L-THA, and D-EHA were confirmed by Silica Gel TLC using 7:1:2 (*v*/*v*/*v*) ethanol/28 % aqueous ammonia/water as a mobile phase. After developing the TLC plates, compounds were visualized by using a Ninhydrin Spray (Wako Pure Chemical Industries), followed by heating.

High-performance liquid chromatography For chiral analysis of amino acids, 2,3,4,6-tetra-*O*-acetyl-β-D-glucopyranosyl isothiocyanate (GITC) was used for the amino acid derivatization. In a GITC derivatization procedure, 0.1 mL of 0.2 % (*w*/*v*) GITC (dissolved in acetonitrile) and 0.02 mL of 2 % (*v*/*v*) triethylamine (dissolved in water) were added to 0.01 mL of reaction samples that were subsequently diluted with acetonitrile to make a total volume of 0.2 mL. The resulting solution was allowed to stand for 30 min at 30 °C. The amino acid derivatives were analyzed using HPLC at a flow rate of 1.0 mL min^{-1} with a CAPCELL PAK C18 MGIII column (4.6×250 mm; Shiseido Company, Ltd., Tokyo, Japan) at 40 °C. Thirty percent (*v*/*v*) methanol or 35 % (*v*/*v*) methanol in water (pH 2.5 adjusted with H_3PO_4) was used as the mobile phase for the analysis of DL-THA or DL-EHA, respectively. Detection was done with a UV detector tuned at 250 nm. The enantiomeric excess (*e.e.*) was calculated from the peak areas of the stereoisomers.

Amino acid analyzer Total concentration of DL-THA or DL-EHA in the reaction mixture was determined with a JLC-500S amino acid analyzer (JEOL, Ltd., Tokyo, Japan).

Nuclear magnetic resonance spectroscopy All NMR spectra were recorded on a Bruker AMX-500 spectrometer (Bruker Corporation, Billerica, MA, ^1H NMR—500 MHz; ^{13}C NMR—125 MHz). Samples taken for the analysis were dissolved in deuterium oxide (D_2O). Chemical shifts were determined relative to the reference signal of an external 3-(trimethylsilyl)propionic-2,2,3,3-d_4 acid (TSP; δ_H, 0 ppm; δ_C, 0 ppm).

Results

Overall structure of D-*threo*-3-hydroxyaspartate dehydratase

The crystal structure of D-THA DH was determined in the substrate-free form at a resolution of 1.5 Å. The asymmetric

unit comprises a dimer formed by a head-to-tail association of two monomers (Fig. 2a). Each monomer is divided into N- and C-terminal domains (Fig. 2b). The N-terminal domain (residues 17-257) consists of eight α-helices ($\alpha1$–$\alpha8$) and eight β-strands ($\beta2$–$\beta9$) which constitute a well-known "triosephosphate isomerase (TIM) barrel" fold, providing a binding site for PLP. The first β-strand of the monomer, $\beta1$, does not form the TIM barrel and is a part of the C-terminal domain since $\beta1$ is located at the extreme N-terminus. The C-terminal domain, comprising residues 1–16 and 258–380, is mainly composed of β-strands. All the nine β-strands ($\beta1$ and $\beta10$–$\beta17$) of the domain form a β-sheet in which the strands are arranged in an antiparallel orientation except for $\beta1$ and $\beta16$. This β-sheet creates a six-stranded β-barrel structure in which the strands ($\beta10$–$\beta11$ and $\beta14$–$\beta15$) are arranged in a Greek-key topology. The PLP-binding site is located at the center of the TIM barrel, between two domains. The overall folding topology is typical of a bacterial alanine racemase. Thus, the current structure provides a conclusive evidence that D-THA DH belongs to the fold-type III group of pyridoxal enzymes.

Cofactor-binding site

The active-site pockets harboring PLP are located at the dimer interface, between the TIM barrel of one monomer and the C-terminal domain of the homodimeric partner. Accordingly, residues bound to PLP (Lys43) yield two active sites per dimer. A highly defined electron density was observed for the entire PLP molecule in each active site. The PLP cofactor binds covalently via an imine bond to the ε-amino group of Lys43, forming an internal aldimine (Schiff base) (Figs. 2c and S2a). The Lys residue is also highly conserved in scDSD and chDSD (Ito et al. 2008; Tanaka et al. 2008). The internal aldimine and the guanidine group of Arg141 are within hydrogen-bonding distance of the phenolic O atom of PLP. The phosphate group of PLP is involved in forming hydrogen bonds to the side-chain atoms of the residues Tyr177 and

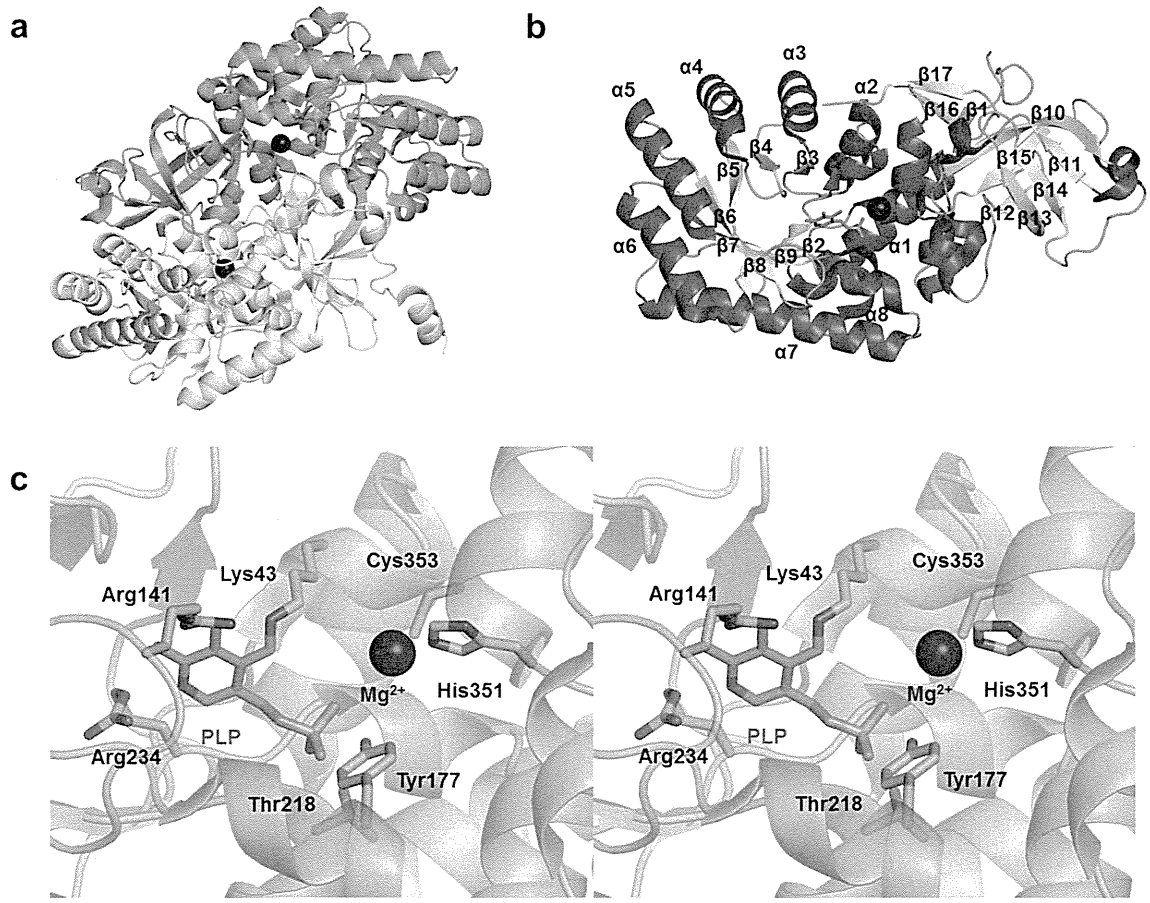

Fig. 2 Structure of D-THA DH from *Delftia* sp. HT23. **a** Ribbon diagram of the dimeric structure where one of the monomers is colored in *green* and the other in *yellow*. The PLP cofactor is shown as a *stick model colored in magenta*, and the Mg^{2+} between side chains of His351 and Cys353 is shown as a *sphere in blue*. **b** Ribbon diagram of the monomeric structure. The α-helices and β-strands and loops are colored in *red*, *yellow*, and *green*, respectively. The α-helices and β-strands are labeled numerically from the N- to C-terminus ($\alpha1$–$\alpha8$ and $\beta1$–$\beta17$). **c** Stereo view showing the cofactor-binding site of D-THA DH in the substrate-free form. Side chains interacting with PLP and Mg^{2+} are shown as *sticks* and labeled. The surrounding polypeptide chain is represented as a *semi-transparent ribbon diagram colored in green*

Thr218 and the main-chain atoms of the residues Thr218, Gly236, and Val237. The pyridine ring of PLP makes a hydrogen bond between its nitrogen atom and the guanidine group of Arg234.

We observed a strong electron density peak between side chains of His351 and Cys353 in each subunit. The electron density was assigned as fully occupied Mg^{2+}, and the model was refined with the reasonable B-factor values comparable to those of nearby residues. Mg^{2+} was probably bound due to the high concentration of $MgCl_2$ (200 mM) in the crystallization solution. The metal-binding site is a part of the C-terminal domain and is formed by His351 and Cys353, which coordinate the metal ion through the N-ε atom of the imidazole ring and the thiol group, respectively (Figs. 2c and S2a). In addition to the two residues, four water molecules complete the octahedral coordination of the Mg^{2+}. The PLP is located near Mg^{2+}, and its phosphate group lies at a distance of about ~5 Å from the metal center. The sequence comparison of D-THA DH with scDSD and chDSD demonstrates that the His and Cys residues coordinating the metal ion are well conserved in these proteins (Ito et al. 2008; Tanaka et al. 2008). All the related proteins show a strong dependency on Zn^{2+}, while D-THA DH works with a various divalent cations including Mg^{2+} as discussed later (Fig. S3).

D-*erythro*-3-hydroxyaspartate (inhibitor)-binding mode of D-*threo*-3-hydroxyaspartate dehydratase

Our previous work has revealed that the specific activity of D-THA DH toward D-EHA is below the limits of detection. D-EHA inhibits D-THA DH with the K_i value of 0.114 mM, determined by replotting the slopes of the Lineweaver-Burk plots. Considering both the results, it can be concluded that D-THA DH has a significant binding affinity toward D-EHA but does not recognize it as a substrate. To elucidate how D-EHA binds in the active site of D-THA DH, its structure was determined in the presence of D-EHA. The structure was determined to a resolution of 1.5 Å, and a clear electron density map was observed for the whole D-EHA molecule bound to the PLP cofactor. The active site of each subunit includes a D-EHA molecule and two Mg^{2+} (Fig. 3). One Mg^{2+} is located between His351 and Cys353 as described in the ligand-free structure. The other Mg^{2+} is chelated by the β-carboxyl O atom and the β-hydroxyl O atom of D-EHA, forming a D-EHA-Mg^{2+} complex. Thus, the latter Mg^{2+} is most likely accompanied by the presence of a ligand containing a β-carboxyl and β-hydroxyl group. Electron density allowed the modeling of a covalent linkage between the C4A atom of PLP and the α-amino group of D-EHA, generating an external aldimine bond. The internal aldimine linkage between the cofactor and Lys43 appeared to be broken in the electron density (Fig. S2b). Although significant structural differences were not observed, an approximately 16° rotation of the cofactor pyridine ring was seen accompanied by the Schiff base interchange. The α-carboxyl group of D-EHA forms hydrogen bonds to the guanidine group of Arg141 from the PLP-binding subunit and the main-chain N atom of Gln319 from the neighboring subunit. Note that the β-hydroxyl O atom of D-EHA is located at a distance of 5.5 Å from the Mg^{2+} positioned between His351 and Cys353. Crystallographic studies of chDSD have demonstrated that the Zn^{2+} sandwiched by His347 and Cys349 probably comes in contact with the β-hydroxyl group of D-serine and may have a catalytic role in leaving the hydroxyl as a water molecule (Tanaka et al. 2011). Therefore, the spatial arrangement of the hydroxyl group that lies far from the enzyme-coordinated Mg^{2+} presumably results in loss of the dehydration activity against D-EHA.

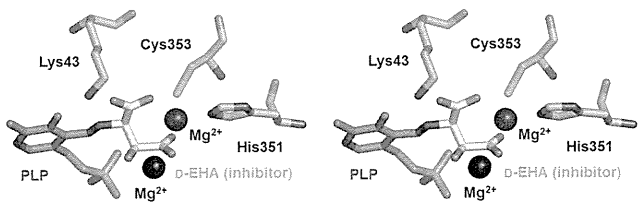

Fig. 3 Stereo view of the active-site structure of D-THA DH with the bound inhibitor (D-EHA). The functionally important residues (in *green*), PLP (in *magenta*), and bound D-EHA (in *yellow*) are shown as *sticks* and labeled. Mg^{2+} is shown as *blue spheres*

Insights into the substrate binding

To elucidate the structural mechanism of the substrate recognition of D-THA DH, we have attempted to determine the structure of inactive mutant in complex with its substrate. We generated the H351A and C353A mutants of D-THA DH and performed an enzyme assay using D-THA and L-EHA as substrates. The results demonstrated that both H351A and C353A mutations significantly decrease the activity toward D-THA and L-EHA (Table 2), similar to the results obtained with

Table 2 Specific activities of the wild-type and mutants of D-THA DH

Variant	3-Hydroxyaspartate dehydratase activity (μmol/min/mg protein)	
	D-THA	L-EHA
Wild-type	21.1±0.79 (100)	16.1±0.18 (100)
H351A	0.12±0.001 (0.57)	0.46±0.006 (2.86)
C353A	ND	ND

Values in parentheses refer to the relative activity (%)

ND not detected (less than 0.01 μmol/min/mg protein)

scDSD (Ito et al. 2012). In particular, the specific activity of C353A mutant toward D-THA and L-EHA was below the detection limit, indicating that Cys353 is a key determinant of the enzymatic activity of D-THA DH. We have first determined the crystal structures of H351A and C353A in the substrate-free form at resolutions of 1.7 and 1.55 Å, respectively. Crystals of each mutant were obtained under the same crystallization condition as for the wild-type D-THA DH. In the structure of the H351A mutant, Mg^{2+} occupies a position near the side chain of Cys353. It is coordinated in an octahedral geometry by the thiol S atom of Cys353 and five water molecules, positioned from the metal center at distances of about 3.6 and 2.0–2.1 Å, respectively. These observations indicate that the H351A mutant utilizes only one cysteine residue for the metal binding. In contrast, no electron density for a metal bound to the active-site pocket was observed in the structure of C353A mutant. It is thus suggested that the Mg^{2+} is held by the side chain of Cys353 rather than by that of His351. Even in the absence of the metal, the structure of C353A mutant displays a conformation similar to the wild-type enzyme. It should also be noted that the short soak of wild-type D-THA DH crystal into the metal-free solution led to the elimination of Mg^{2+} from the active site (Table 1; PDB code, 3WQF). These suggest a low binding affinity of Mg^{2+} and that the Mg^{2+} is not required for the structural stabilization of the enzyme.

Structures of the H351A cocrystallized with D-THA and L-EHA were also determined at resolutions of 1.8 and 1.9 Å, respectively. The covalent linkages appear to be formed between the PLP cofactor and the α-amino groups of substrates from the electron density map. Attempts to solve the crystal structures of the C353A in complex with D-THA and L-EHA were not successful. Mg^{2+} could not bind to the active site of C353A mutant, leading to a significant decrease in its substrate-binding affinity. The electron density map of the structure of H351A cocrystallized with D-THA unexpectedly showed that the N-C^{α}-C^{β}-C^{γ} of a bound substrate is roughly coplanar with the lacking β-hydroxyl group. This prompted us to build a model of 2-amino maleic acid (Fig. 4a, b). 2-Amino maleic acid is a likely product of the dehydration of D-THA, and thus, the current complex structure represents its intermediate state in the catalytic cycle of D-THA DH (Fig. 5). The water molecule (Wat709A/Wat712B) located near the intermediate C^{β} atom at a distance of 2.0 Å was probably generated by the dehydratase reaction catalyzed by the H351A mutant. Water also interacts with the liberated ε-amino group of Lys43 (2.9 Å), the phosphate group of PLP (2.5 Å), and the

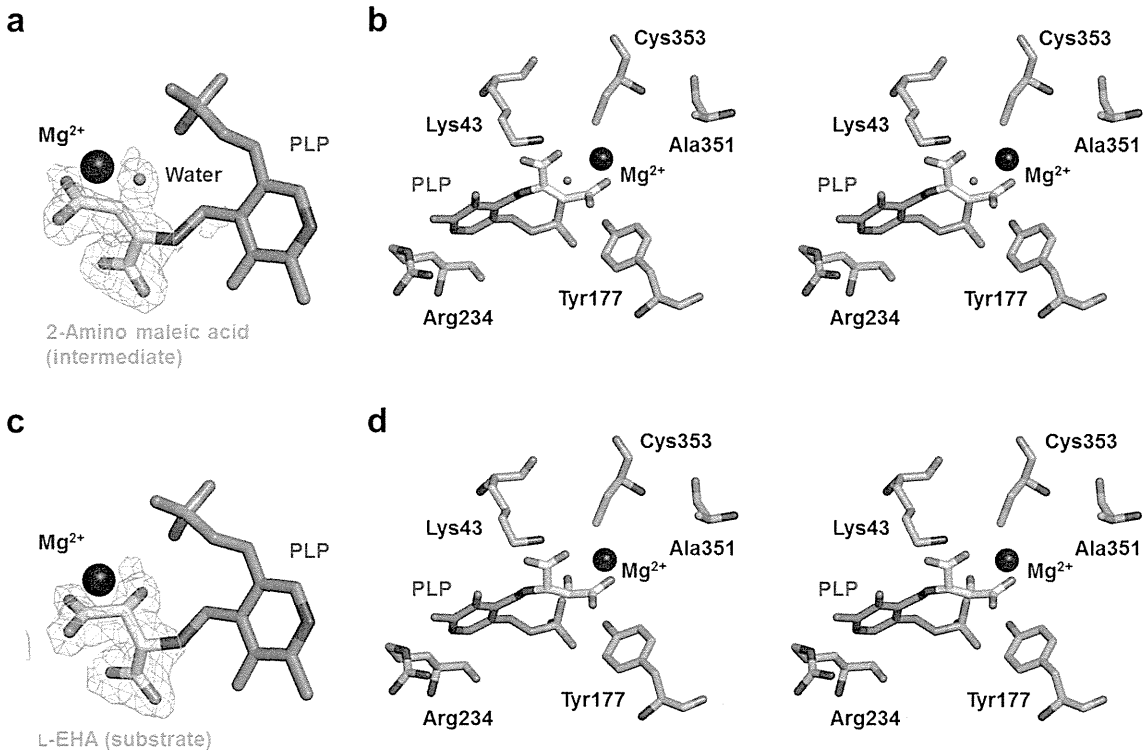

Fig. 4 2-Amino maleic acid and L-EHA binding to the H351A mutant of D-THA DH. **a** An mF_o-DF_c omit map for bound 2-amino maleic acid and the water molecule (Wat709A/Wat712B) is shown. The map was contoured at the 2.8σ level. **b** Stereo view representation of the active-site structure of the H351A mutant with the reaction intermediate 2-amino maleic acid. The functionally important residues including mutational residue Ala351 (in *green*), PLP (in *magenta*), and 2-amino maleic acid (in *yellow*) are shown as *sticks* and labeled. The nearest water molecule (Wat709A/Wat712B) from the intermediate C^{β} atom is also shown in *red* and Mg^{2+} in *blue*. **c** An mF_o-DF_c omit map for bound L-EHA is shown. The map was contoured at 2.6σ level. **d** Stereo view representation of the active-site structure of the H351A mutant with substrate L-EHA. This image was prepared in the same way and in the same orientation as that of **b**

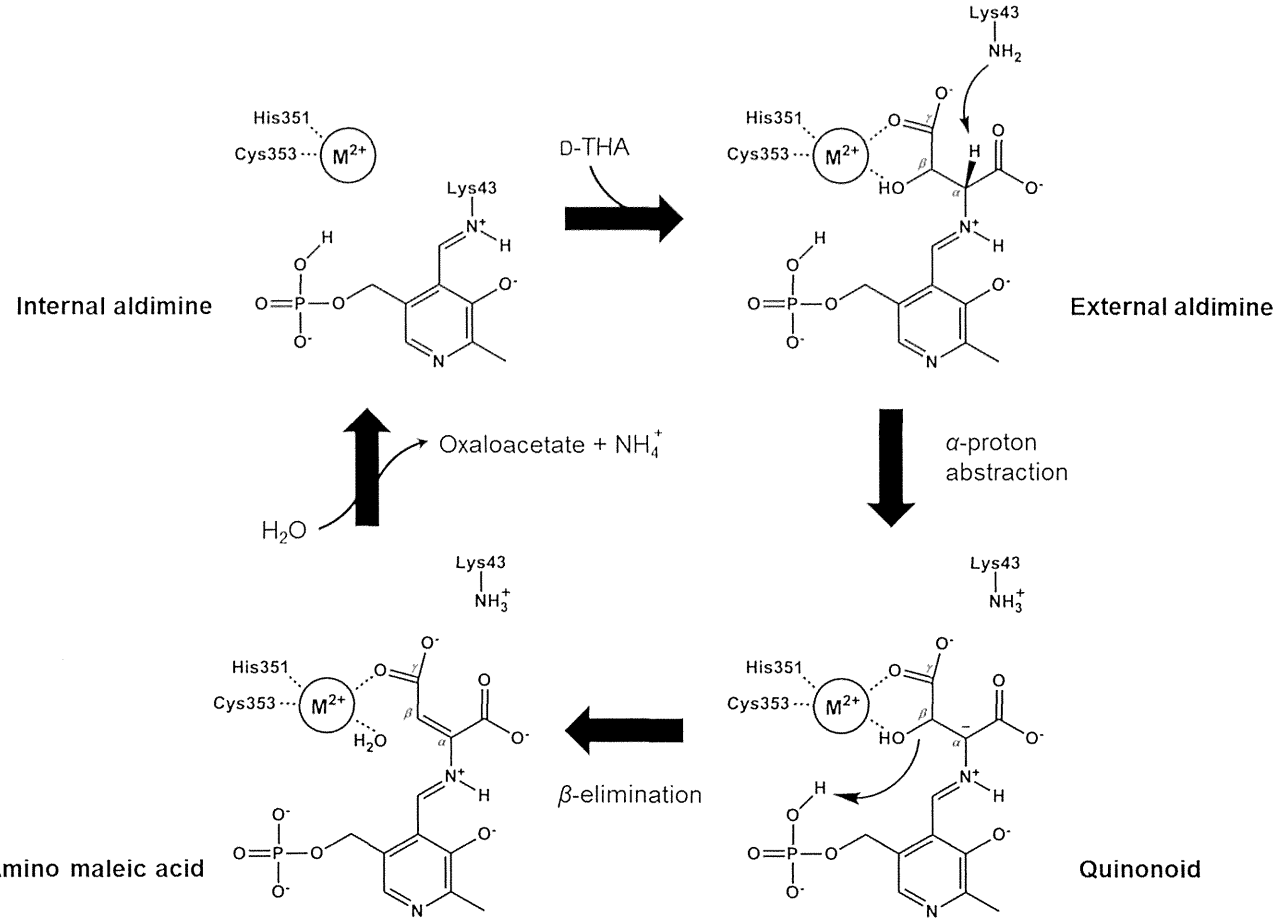

Fig. 5 Proposed catalytic cycle of D-THA DH based on the structure of the H351A mutant in complex with 2-amino maleic acid. Initial addition of the substrate converts lysine-PLP (internal aldimine) to PLP-D-THA (external aldimine). Next, proton abstraction from the α-carbon of bound D-THA occurs by Lys43 (Arg141 and/or His172 in the case of L-EHA) to generate a quinonoid intermediate. The PLP-2-amino maleic acid complex is subsequently generated by the β-elimination reaction promoted by the interaction between the hydroxyl O atom and the active-site metal ion (represented as M^{2+}). The protonated phosphate of PLP acts as an acid to donate its proton to the hydroxyl, which is then released as water. Finally, regeneration of the internal aldimine linkage and nonenzymatic hydrolysis of the resulting free imine/enamine release oxaloacetate and ammonia

cysteine-coordinated Mg^{2+} (2.3 Å). These observations indicate that the C^{β}-OH orientation of D-THA would be an important factor contributing to the substrate recognition of D-THA DH. In addition, Mg^{2+} might directly interact with the β-hydroxyl group of D-THA to promote the dehydration reaction. Not only D-THA but also L-EHA is a good substrate for D-THA DH (Maeda et al. 2010). In the structure of H351A cocrystallized with L-EHA, the electron density corresponding to L-EHA was clearly visible (Fig. 4c, d). The hydroxyl O atom of L-EHA occupies roughly the same position as Wat709A/Wat712B liberated from D-THA in the reaction intermediate complex and is also in direct contact with the Mg^{2+}. Thus, the substrate stereospecificity of D-THA DH is determined by the C^{β}-OH orientation of the substrate at the active site.

In summary, we have determined three complex structures that shed light on the 3-hydroxyaspartate recognition mechanism of D-THA DH: the wild-type enzyme in complex with D-EHA, the H351A mutant in complex with 2-amino maleic acid originating from D-THA, and the H351A mutant in complex with L-EHA. Obtaining the complex structure with L-THA was tried with both the wild-type and the H351A mutant enzymes; however, there was no visible electron density for L-THA in the active-site pockets. This was explained by the high K_m value of D-THA DH for L-THA (K_m=6.16 mM; Maeda et al. 2010). Interestingly, the current structural studies revealed that chirality at the C^{β} position of 3-hydroxyaspartate (3*R*) can be well recognized by D-THA DH as substrates. The C^{β} configuration of D-THA superimposed well onto that of L-EHA in the present models, which is associated with the high levels of activities against D-THA and L-EHA. Thus, the active-site conformation of D-THA DH would be compatible with the 3*R* configuration of 3-hydroxyaspartate. This finding provides an explanation for the efficient production of optically pure 3-hydroxyaspartate having the 3*S* configuration as described below.

Biocatalytic preparation of L-*threo*-3-hydroxyaspartate from DL-*threo*-3-hydroxyaspartate using D-*threo*-3-hydroxyaspartate dehydratase

We have developed a novel method for producing optically pure L-THA, which is (2*S*,3*S*) form of 3-hydroxyaspartate and a promising intermediate for the synthesis of L-TBOA, an important compound in understanding the regulatory functions of glutamate transporters in the human brain (Shimamoto 2008). Enzyme kinetics and the structural analysis have indicated that D-THA DH is useful in the dehydratase-catalyzed optical resolution of DL-THA. Therefore, we evaluated the biocatalytic preparation of optically pure L-THA by using purified D-THA DH. After 6 h, the enantiomeric excess (*e.e.*) of L-THA in the reaction mixture reached >99 % as calculated from the peak areas in the HPLC analysis (Fig. 6a). In addition, the total concentration of DL-THA determined with an amino acid analyzer decreased to about half the initial value at the same time (Fig. S4). These results indicate that D-THA in the racemate solution was enantioselectively converted to oxaloacetate and ammonia by the enzymatic reaction. Remaining L-THA in the reaction product was crystallized under the acidified condition (pH 2.0). The resulting residue was an enantiopure L-THA as determined by HPLC analysis (Fig. S5). The isolation yield as dry weight was 38.9 % against the amount of DL-THA initially added to the reaction mixture. Moreover, chemical purity of the final product was verified by NMR analysis, and it showed the following signals (Fig. S6): ^{1}H NMR (500 MHz, TSP=0 ppm)—3.98 (1H, d, J=1.8 Hz) and 4.52 ppm (1H, d, J=1.8 Hz); ^{13}C NMR (125 MHz, TSP=0 ppm)—60.02, 74.08, 176.47, and 179.77 ppm. These signals indicate the *threo* isomer of 3-hydroxyaspartate.

Biocatalytic preparation of D-*erythro*-3-hydroxyaspartate from DL-*erythro*-3-hydroxyaspartate by D-*threo*-3-hydroxyaspartate dehydratase

Similarly, biocatalytic preparation of optically pure D-EHA, which is (2*R*,3*S*)-3-hydroxyaspartate, from DL-EHA, was achieved by using purified D-THA DH. The derivative of D-EHA, D-*erythro*-*β*-benzyloxyaspartate (D-EBOA), was also found to act as a blocker for EAATs although the effect was relatively weak (Shimamoto et al. 2000). After 10 h of bioconversion, the reaction mixture contained only the D-enantiomer of *erythro*-3-hydroxyaspartate with >99 % *e.e.* and 48.9 % of the isolated yield (Figs. 6b and S7). The result of NMR signals verified the chemical purity of the final product as *erythro* isomer of 3-hydroxyaspartate (Fig. S8): ^{1}H NMR (500 MHz, TSP=0 ppm)—4.00 (1H, d, J=3.6 Hz) and 4.33 ppm (1H, d, J=3.6 Hz); ^{13}C NMR (125 MHz, TSP=0 ppm)—60.86, 74.47, 175.12, and 179.16 ppm.

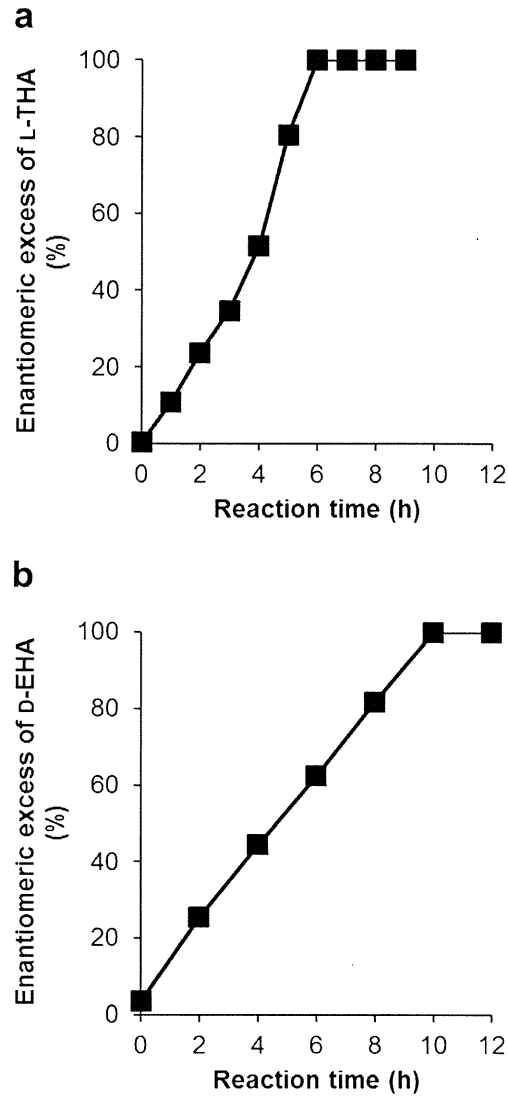

Fig. 6 Optically pure production of L-THA and D-EHA. **a** Biocatalytic preparation of L-THA from DL-THA by purified D-THA DH. The reaction mixture consisted of 100 mM Tris-HCl buffer (pH 8.0), 0.01 mM PLP, 0.1 mM $MnCl_2$, 200 mM DL-THA, and 0.66 mg of the enzyme in a total volume of 100 mL. During incubation, the D-form and L-form of 3-hydroxyaspartate in the reaction mixture were monitored using HPLC. The enantiomeric excess (*e.e.*) was calculated from the peak areas of the stereoisomers. **b** Biocatalytic preparation of D-EHA from DL-EHA by purified D-THA DH. The experiment and calculation were performed with the same procedure as for the production of L-THA except for an enzyme amount of 0.87 mg

Discussion

Structure comparison with D-serine dehydratase from chicken kidney

Pairwise structure comparison using the *DALI* server (Holm and Park 2000) showed that D-THA DH is structurally homologous to D-serine dehydratase from chicken kidney (chDSD; Tanaka et al. 2011; PDB code, 3ANU; Z score, 45.2; RMSD,

1.9 Å for 358C$^{\alpha}$ atoms; sequence identity for fit regions, 37 %). Although the overall folds of D-THA DH and chDSD are identical, there are apparent differences that need to be discussed. The first difference is the oligomerization state in the solution. Tanaka et al. based on the gel filtration chromatography results have reported that chDSD forms a dimer in the solution. Even though crystallographic studies of chDSD demonstrate that the asymmetric unit comprises a single monomer, the biological assembly is assumed head-to-tail dimer. It is created by a crystallographic 2-fold axis involving large and hydrophilic interface between the subunits. In contrast to chDSD, judging from its apparent molecular mass analyzed by the gel filtration, D-THA DH is a monomeric enzyme as previously reported (Maeda et al. 2010). However, as shown in the present study, all the crystal forms of D-THA DH have the head-to-tail dimer in the asymmetric unit, similar to the biological assembly of chDSD. The dimeric state of D-THA DH revealed that the amino acid residues Asn318-His321, which form a loop in the C-terminal domain, contact neighboring PLP-binding pockets and include a Gln319 that is expected to be utilized for D-EHA, D-THA, and L-EHA binding. Each domain is also responsible for the dimerization through hydrogen bonds. Therefore, the current symmetric dimer is likely to be one of the possible conformational states of D-THA DH and the crystal lattice forces may stabilize this conformation. The second difference is found in the arrangement of residues that directly interact with the pyridine nitrogen, designated as N1. The structure of chDSD revealed that the side chain of Tyr174 is within hydrogen-bonding distance of N1. This environment may preclude the protonation of N1 that possibly functions as a driving force for the catalysis of transamination. Therefore, the N1-unprotonated state of chDSD is needed for the catalysis of β-elimination and for avoiding other PLP-catalyzed reactions. Likewise, although the Tyr residue is substituted with Leu170 in D-THA DH based on the primary structure alignment, the alternate Arg residue at position 234 is hydrogen bonded to N1, thereby preventing proton transfer to N1 due to the high pK_a value of the arginine side chain (~12.5 in water).

In this structural study, Mg^{2+} was observed between the side chains of His351 and Cys353, probably due to artificial crystallization solution containing 200 mM $MgCl_2$. Although it is uncommon that Mg^{2+} is coordinated by imidazole and thiol ligands, the atomic coordinates and the B-factor values were reasonably refined without extra F_o-F_c density map, indicating that the bound metal is conclusively Mg^{2+}. The Mg^{2+}-free structure (Table 1; PDB code, 3WQF) also suggests that D-THA DH has a low affinity for Mg^{2+}. To examine which metals occupy the active site prior to crystallization, an inductively coupled plasma mass spectrometry (ICP-MS) analysis was conducted on purified D-THA DH. The results showed that a large amount of Zn^{2+} was detected in the purified enzyme (Fig. S9). A relatively high content of Ni^{2+} and Co^{2+} was also detected after Ni^{2+}- and Co^{2+}-affinity purification, respectively. Therefore, it can be concluded that D-THA DH naturally contains Zn^{2+}, but under the given experimental conditions, the substitution of Zn^{2+} for other metals takes place easily. Tanaka and coworkers have reported that chDSD naturally possesses Zn^{2+} based on its X-ray structure and only Mn^{2+} can partially substitute Zn^{2+} for the catalytic activity against D-serine. In contrast, we have previously reported that D-THA DH works with a various divalent cations such as Co^{2+}, Mn^{2+}, Ni^{2+}, Ca^{2+}, Zn^{2+}, and Fe^{2+} (Maeda et al. 2010). Furthermore, addition of $MgCl_2$ to the enzyme solution after treatment with ethylenediaminetetraacetic acid (EDTA) gave a low but significant recovery of the specific activity of D-THA DH from 0.1 to 1.2 μmol/min/mg protein (Fig. S3). This clearly shows that the Mg^{2+} is functional and is involved in the enzymatic activity.

Insights into the catalytic mechanism and the substrate stereoselectivity

Note that the substitution of alanine for Cys353 precludes the binding of Mg^{2+} to D-THA DH (Table 1; PDB code, 3WQC). Structure of C353A mutant also showed no binding affinity toward D-EHA, D-THA, and L-EHA (data not shown). Considering these results, it can be concluded that the substrate/inhibitor-binding affinities of D-THA DH are greatly decreased by the absence of the metal. In contrast, crystallographic analyses have revealed that the pretreatment of EDTA allows chDSD to bind with D-serine even in the absence of Zn^{2+}. This suggests that chDSD does not require metal for the initial occurrence of the Schiff base interchange from lysine-PLP to PLP-substrate.

On the basis of the X-ray structure of H351A cocrystallized with D-THA/L-EHA, a possible mechanism for the catalytic reaction of D-THA DH has been proposed (Fig. 5). Initially, the substrate covalently binds to the PLP molecule in each active-site pocket of the dimeric state of D-THA DH. Metal ion is also in direct contact with the β-carboxyl and β-hydroxyl O atoms, presumably playing a role in the stabilization of the bound substrate during the catalytic reaction. Upon abstracting a proton from the α-carbon of D-THA by Lys43 to generate a quinonoid resonance structure, the β-elimination reaction occurs by a proton donation to the substrate hydroxyl group. In previous structural studies on chDSD, the reported distance between the NZ atom of the Lys45 and the β-hydroxyl of D-serine was an optimal distance (3.2 Å) for the proton donation, suggesting that the abstracted α-proton could be transferred to the substrate hydroxyl via the lysine residue as an acid/base catalyst (Tanaka et al. 2011). In contrast, the current complex structures of the H351A mutant indicate that another candidate, a phosphate group of PLP, is located in the proper position contributing to the β-elimination reaction. We can assume that the protonated phosphate O atom acts as a

general acid to donate a proton to the leaving hydroxyl group of the substrate. Indeed, the side chain of Tyr177 is in contact with the phosphate O atom, thus maintaining the protonation state in transferring proton throughout the reaction. Also, the distances from the hydroxyl group of substrate L-EHA to the ε-amino group of Lys43 (2.8 Å) and the phosphate group of PLP (2.6 Å) are shorter than the corresponding distances from the hydroxyl group of inhibitor D-EHA to the ε-amino group (5.8 Å) and the phosphate (5.7 Å). Considering that the ε-amino group of Lys43 exhibits conformational dynamics in response to the catalytic cycle, the association between the protonated phosphate group and the substrate hydroxyl is more responsible for leaving the hydroxyl group as a water molecule. We observed the PLP-2-amino maleic acid complex as the subsequent intermediate. An imine/enamine released after the internal Schiff base regeneration is thought to be hydrolyzed nonenzymatically. Thus, tautomeric change of free 2-amino maleic acid into 2-imino succinic acid and subsequent hydrolysis eliminate ammonia from the imine to give oxaloacetate.

C^{α}-H deprotonation is commonly carried out by the ε-amino group of a lysine that is liberated from the internal aldimine with PLP (Toney 2005). In this study, the ε-amino group of Lys43 could access the α-proton of D-THA, while it could not interact with that of L-EHA. Alternatively, side chains of Arg141 and His172 are situated close to the α-proton of L-EHA and would play a role in the proton abstraction. Our previous kinetic analysis based on the k_{cat}/K_m values indicates that D-THA DH has 2.6-fold higher binding affinity for L-EHA than for D-THA, thereby acting more effectively on L-EHA (Maeda et al. 2010). Since the only difference between D-THA and L-EHA is the chirality at the C^{α} position (Fig. 1), it is suggested that the α-proton abstraction from L-EHA by Arg141 and/or His172 might increase the dehydratase activity. This raises the possibility that D-THA DH possesses the epimerase activity between D-THA and L-EHA. However, the HPLC chromatograms can preclude this possibility.

Synthesis of optically pure 3-hydroxyaspartate using D-*threo*-3-hydroxyaspartate dehydratase

In this study, we have developed a novel synthetic approach leading to L-THA and D-EHA via the dehydratase-catalyzed optical resolution. The separation of L-THA from the corresponding racemate, DL-THA, was achieved by converting D-THA into oxaloacetate using recombinant D-THA DH. Additionally, L-EHA also serves as a good substrate; therefore, D-THA DH was also used for the synthesis of D-EHA starting from DL-EHA. To date, there have been no published studies on an enzymatic optical resolution of racemic 3-hydroxyaspartates, although convenient synthetic routes for DL-THA and DL-EHA starting from (±)-*trans*-epoxysuccinic acid were established many years ago (Kaneko and Katsura 1963). Thus, our data confirm for the first time the utility of D-THA DH as a biocatalyst for the resolution of DL-*threo*/*erythro*-3-hydroxyaspartate.

The racemic mixture contains both enantiomers in equal amounts, and thus, the maximum yield in an optical resolution is 50 %. Considering this theoretical maximum, the synthetic approaches are quite efficient as judged from the isolated yields of L-THA and D-EHA. However, D-THA DH was found to possess a slight activity against L-THA (Maeda et al. 2010), resulting in a lower yield of L-THA (38.9 %) compared to D-EHA (48.9 %). There is a need for further studies to create the mutant enzyme showing no activity on L-THA. In addition, the reaction time of L-EHA degradation was longer than expected. This is likely due to inhibition of the dehydratase by binding of D-EHA, which is the remaining product. Thus, a short reaction time requires use of the mutant enzyme capable of overcoming the inhibition, which could be accomplished by the structure-based engineering of D-THA DH whose structure in complex with D-EHA has been reported here.

We confirmed the final products as pure L-THA and D-EHA by analyzing them with TLC, HPLC, and NMR spectroscopy. We were able to isolate pure compounds directly by recrystallization of the reaction mixtures, utilizing the lower solubility of 3-hydroxyaspartate in acidic water (pH 2.0) compared to oxaloacetate and ammonia. Therefore, this synthetic approach has an advantage for obtaining pure products without any chromatographic purification. It is efficient and friendly to the environment because of minimal or no use of organic solvents.

Strieker et al. (2008) reported that a single mutant of asparagine oxygenase ($AsnO_{D241N}$) from *S. coelicolor* catalyzes one-step hydroxylation of L-aspartate to produce L-THA. The bioconversion represents one of the simplest strategies for preparing L-THA from a low-cost material. However, it is important to note that 1.16 g of the isolated yield of L-THA per 100 mL of the reaction mixture was achieved in this study, which is a considerable amount compared to the production data of Strieker et al. (14.8 mg of the isolated yield per 10 mL of the reaction mixture). Strieker and coworkers have also reported that the conversion reaction was carried out under optimized conditions including a low temperature of 16 °C most probably due to the reduced enzyme stability of $AsnO_{D241N}$. In contrast, D-THA DH was found to be thermally stable up to 45 °C (Fig. S10), which would be more acceptable for industrial-scale reactions demanding moderate- to high-temperature conditions.

Acknowledgments Authors would like to thank Dr. Eri Fukushi and Mr. Yusuke Takata of the GC-MS & NMR Laboratory (Research Faculty of Agriculture, Hokkaido University) for assistance with the NMR spectral measurements. We are grateful to Dr. Toshihiro Watanabe (Research Faculty of Agriculture, Hokkaido University) for conducting the ICP-MS analysis. Authors also acknowledge the technical staff at Photon Factory

(PF) for their kind support in the X-ray diffraction experiments. This work was financially supported in part by a grant-in-aid from the Institute for Fermentation, Osaka (IFO). Synchrotron radiation experiments were conducted under the approval of 2012G576 at PF.

References

Antolini L, Bucciarelli M, Caselli E, Davoli P, Forni A, Moretti I, Prati F, Torre G (1997) Stereoselective synthesis of *erythro* β-substituted aspartates. J Org Chem 62:8784–8789. doi:10.1021/jo971285+

Arriza JL, Fairman WA, Wadiche JI, Murdoch GH, Kavanaugh MP, Amara SG (1994) Functional comparisons of three glutamate transporter subtypes cloned from human motor cortex. J Neurosci 14: 5559–5569

Arriza JL, Eliasof S, Kavanaugh MP, Amara SG (1997) Excitatory amino acid transporter 5, a retinal glutamate transporter coupled to a chloride conductance. Proc Natl Acad Sci U S A 94:4155–4160

Battye TGG, Kontogiannis L, Johnson O, Powell HR, Leslie AGW (2011) iMOSFLM: a new graphical interface for diffraction-image processing with MOSFLM. Acta Crystallogr Sect D: Biol Crystallogr 67:271–281. doi:10.1107/S0907444910048675

Bionda N, Cudic M, Barisic L, Stawikowski M, Stawikowska R, Binetti D, Cudic P (2012) A practical synthesis of N^{α}-Fmoc protected L-*threo*-β-hydroxyaspartic acid derivatives for coupling via α- or β-carboxylic group. Amino Acids 42:285–293. doi:10.1007/s00726-010-0806-x

Cardillo G, Gentilucci L, Tolomelli A, Tomasini C (1999) A practical method for the synthesis of β-amino α-hydroxy acids. Synthesis of enantiomerically pure hydroxyaspartic acid and isoserine. Synlett 11:1727–1730. doi:10.1055/s-1999-2927

DeLano WL (2002) PyMOL. http://www.pymol.org/. Accessed 19 December 2014

Deng J, Hamada Y, Shioiri T (1995) Total synthesis of alterobactin A, a super siderophore from an open-ocean bacterium. J Am Chem Soc 117:7824–7825. doi:10.1021/ja00134a035

Eliot AC, Kirsch JF (2004) Pyridoxal phosphate enzymes: mechanistic, structural, and evolutionary considerations. Annu Rev Biochem 73: 383–415. doi:10.1146/annurev.biochem.73.011303.074021

Emsley P, Cowtan K (2004) Coot: model-building tools for molecular graphics. Acta Crystallogr Sect D: Biol Crystallogr 60:2126–2132. doi:10.1107/S0907444904019158

Hara R, Kino K (2010) Industrial production of *threo*-3-hydroxy-L-aspartic acid using *Escherichia coli* resting cells. J Biotechnol 150S:373. doi:10.1016/j.jbiotec.2010.09.450

Holm L, Park J (2000) DaliLite workbench for protein structure comparison. Bioinformatics 16:566–567. doi:10.1093/bioinformatics/16.6.566

Ito T, Hemmi H, Kataoka K, Mukai Y, Yoshimura T (2008) A novel zinc-dependent D-serine dehydratase from *Saccharomyces cerevisiae*. Biochem J 409:399–406. doi:10.1042/BJ20070642

Ito T, Koga K, Hemmi H, Yoshimura T (2012) Role of zinc ion for catalytic activity in D-serine dehydratase from *Saccharomyces cerevisiae*. FEBS J 279:612–624. doi:10.1111/j.1742-4658.2011.08451.x

Kaneko T, Katsura H (1963) The synthesis of four optical isomers of β-hydroxyaspartic acid. Bull Chem Soc Jpn 36:899–903. doi:10.1246/bcsj.36.899

Khalaf JK, Datta A (2008) A concise, asymmetric synthesis of (2*R*,3*R*)-3-hydroxyaspartic acid. Amino Acids 35:507–510. doi:10.1007/s00726-007-0595-z

Liu JQ, Dairi T, Itoh N, Kataoka M, Shimizu S (2003) A novel enzyme, D-3-hydroxyaspartate aldolase from *Paracoccus denitrificans* IFO 13301: purification, characterization, and gene cloning. Appl Microbiol Biotechnol 62:53–60. doi:10.1007/s00253-003-1238-2

Maeda T, Takeda Y, Murakami T, Yokota A, Wada M (2010) Purification, characterization and amino acid sequence of a novel enzyme, D-*threo*-3-hydroxyaspartate dehydratase, from *Delftia* sp. HT23. J Biochem 148:705–712. doi:10.1093/jb/mvq106

Matsumoto Y, Yasutake Y, Takeda Y, Tamura T, Yokota A, Wada M (2013) Crystallization and preliminary X-ray diffraction studies of D-*threo*-3-hydroxyaspartate dehydratase isolated from *Delftia* sp. HT23. Acta Crystallogr Sect F: Struct Biol Cryst Commun 69: 1131–1134. doi:10.1107/S1744309113023956

Murakami T, Maeda T, Yokota A, Wada M (2009) Gene cloning and expression of pyridoxal 5′-phosphate-dependent L-*threo*-3-hydroxyaspartate dehydratase from *Pseudomonas* sp. T62, and characterization of the recombinant enzyme. J Biochem 145:661–668. doi:10.1093/jb/mvp023

Murshudov GN, Skubák P, Lebedev AA, Pannu NS, Steiner RA, Nicholls RA, Winn MD, Long F, Vagin AA (2011) REFMAC5 for the refinement of macromolecular crystal structures. Acta Crystallogr Sect D: Biol Crystallogr 67:355–367. doi:10.1107/S0907444911001314

Nakashima N, Tamura T (2004a) A novel system for expressing recombinant proteins over a wide temperature range from 4 to 35 °C. Biotechnol Bioeng 86:136–148. doi:10.1002/bit.20024

Nakashima N, Tamura T (2004b) Isolation and characterization of a rolling-circle-type plasmid from *Rhodococcus erythropolis* and application of the plasmid to multiple-recombinant-protein expression. Appl Environ Microbiol 70:5557–5568. doi:10.1128/AEM.70.9.5557-5568.2004

Otwinowski Z, Minor W (1997) Processing of X-ray diffraction data collected in oscillation mode. Methods Enzymol 276:307–326. doi:10.1016/S0076-6879(97)76066-X

Schneider G, Käck H, Lindqvist Y (2000) The manifold of vitamin B_6 dependent enzymes. Structure 8:R1–R6. doi:10.1016/S0969-2126(00)00085-X

Sheldrick GM (2008) A short history of SHELX. Acta Crystallogr Sect A: Found Crystallogr 64:112–122. doi:10.1107/S0108767307043930

Shigeri Y, Shimamoto K, Yasuda-Kamatani Y, Seal RP, Yumoto N, Nakajima T, Amara SG (2001) Effects of *threo*-β-hydroxyaspartate derivatives on excitatory amino acid transporters (EAAT4 and EAAT5). J Neurochem 79:297–302. doi:10.1046/j.1471-4159.2001.00588.x

Shigeri Y, Seal RP, Shimamoto K (2004) Molecular pharmacology of glutamate transporters, EAATs and VGLUTs. Brain Res Rev 45: 250–265. doi:10.1016/j.brainresrev.2004.04.004

Shimamoto K (2008) Glutamate transporter blockers for elucidation of the function of excitatory neurotransmission systems. Chem Rec 8: 182–199. doi:10.1002/tcr.20145

Shimamoto K, Lebrun B, Yasuda-Kamatani Y, Sakaitani M, Shigeri Y, Yumoto N, Nakajima T (1998) DL-*threo*-β-benzyloxyaspartate, a potent blocker of excitatory amino acid transporters. Mol Pharmacol 53:195–201

Shimamoto K, Shigeri Y, Yasuda-Kamatani Y, Lebrun B, Yumoto N, Nakajima T (2000) Syntheses of optically pure β-hydroxyaspartate derivatives as glutamate transporter blockers. Bioorg Med Chem Lett 10:2407–2410. doi:10.1016/S0960-894X(00)00487-X

Shimamoto K, Sakai R, Takaoka K, Yumoto N, Nakajima T, Amara SG, Shigeri Y (2004) Characterization of novel L-*threo*-β-benzyloxyaspartate derivatives, potent blockers of the glutamate transporters. Mol Pharmacol 65:1008–1015. doi:10.1124/mol.65.4.1008

Strieker M, Essen LO, Walsh CT, Marahiel MA (2008) Non-heme hydroxylase engineering for simple enzymatic synthesis of L-*threo*-hydroxyaspartic acid. ChemBioChem 9:374–376. doi:10.1002/cbic.200700557

Tanaka H, Yamamoto A, Ishida T, Horiike K (2008) D-serine dehydratase from chicken kidney: a vertebral homologue of the cryptic enzyme from *Burkholderia cepacia*. J Biochem 143:49–57. doi:10.1093/jb/mvm203

Tanaka H, Senda M, Venugopalan N, Yamamoto A, Senda T, Ishida T, Horiike K (2011) Crystal structure of a zinc-dependent D-serine dehydratase from chicken kidney. J Biol Chem 286:27548–27558. doi:10.1074/jbc.M110.201160

Terwilliger TC (2000) Maximum-likelihood density modification. Acta Crystallogr Sect D: Biol Crystallogr 56:965–972

Terwilliger TC, Berendzen J (1999) Automated MAD and MIR structure solution. Acta Crystallogr Sect D: Biol Crystallogr 55:849–861. doi:10.1107/S0907444999000839

Toney MD (2005) Reaction specificity in pyridoxal phosphate enzymes. Arch Biochem Biophys 433:279–287. doi:10.1016/j.abb.2004.09.037

Wada M, Matsumoto T, Nakamori S, Sakamoto M, Kataoka M, Liu JQ, Itoh N, Yamada H, Shimizu S (1999) Purification and characterization of a novel enzyme, L-*threo*-3-hydroxyaspartate dehydratase, from *Pseudomonas* sp. T62. FEMS Microbiol Lett 179:147–151

Wada M, Nakamori S, Takagi H (2003) Serine racemase homologue of *Saccharomyces cerevisiae* has L-*threo*-3-hydroxyaspartate dehydratase activity. FEMS Microbiol Lett 225:189–193. doi:10.1016/S0378-1097(03)00484-1

Winn MD, Ballard CC, Cowtan KD, Dodson EJ, Emsley P, Evans PR, Keegan RM, Krissinel EB, Leslie AGW, McCoy A, McNicholas SJ, Murshudov GN, Pannu NS, Potterton EA, Powell HR, Read RJ, Vagin A, Wilson KS (2011) Overview of the CCP4 suite and current developments. Acta Crystallogr Sect D: Biol Crystallogr 67:235–242. doi:10.1107/S0907444910045749

Supplementary Material for *Applied Microbiology and Biotechnology*

Structural insights into the substrate stereospecificity of D-*threo*-3-hydroxyaspartate dehydratase from *Delftia* sp. HT23: a useful enzyme for the synthesis of optically pure L-*threo*- and D-*erythro*-3-hydroxyaspartate

Yu Matsumoto,[a] Yoshiaki Yasutake,[b]* Yuki Takeda,[a] Tomohiro Tamura,[b] Atsushi Yokota,[a] and Masaru Wada[a]*

[a]Laboratory of Microbial Physiology, Research Faculty of Agriculture, Hokkaido University, Kita-9, Nishi-9, Kita-ku, Sapporo 060-8589, Japan, and [b]Bioproduction Research Institute, National Institute of Advanced Industrial Science and Technology (AIST), 2-17-2-1 Tsukisamu-Higashi, Toyohira-ku, Sapporo 062-8517, Japan

*Corresponding authors

Tel: +81-11-857-8514; Fax: +81-11-857-8980; E-mail: y-yasutake@aist.go.jp

Tel: +81-11-706-4185; Fax: +81-11-706-4961; E-mail: wada@chem.agr.hokudai.ac.jp

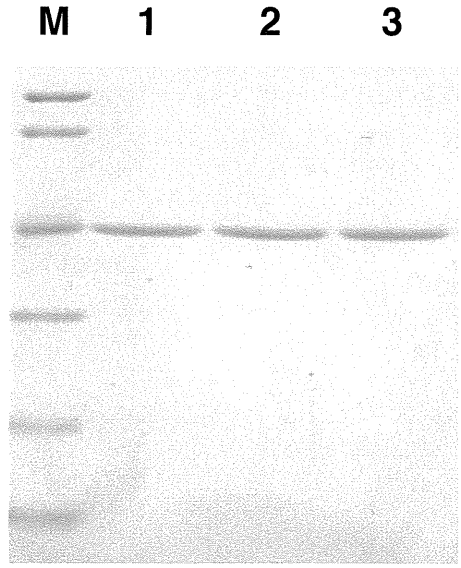

Figure S1 SDS-PAGE of the wild-type and mutants of D-THA DH. *Lanes 1-3* correspond to the wild-type, H351A, and C353A mutants, respectively. *Lane M* contains marker proteins, including (from *top* to *bottom*), phosphorylase (M_r, 97,400), bovine serum albumin (66,300), aldolase (42,400), carbonic anhydrase (30,000), trypsin inhibitor (20,100), and lysozyme (14,400). Gel was stained for protein with Coomassie Brilliant Blue R-250 (Wako Pure Chemical Industries).

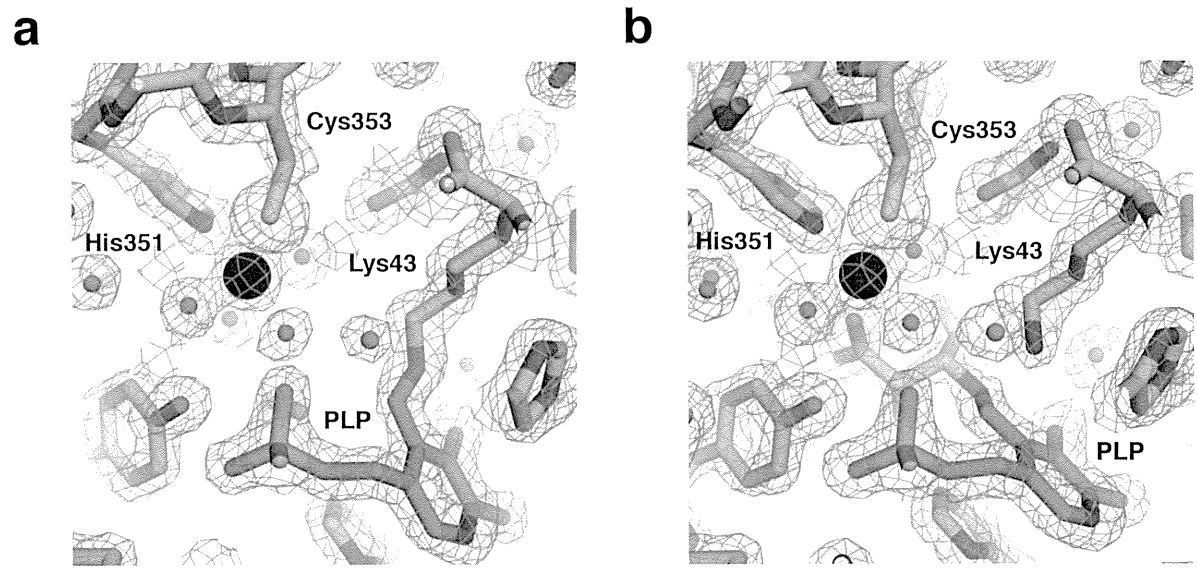

Figure S2 Final 2*mF*o-*DF*c map of the wild-type D-THA DH around active site in (a) substrate-free form (PDB code, 3WQC) and in (b) complex with D-EHA (PDB code, 3WQD), clearly showing the Schiff-base interchange from lysine-PLP to PLP-D-EHA. Each map was shows contours at 1.4σ level.

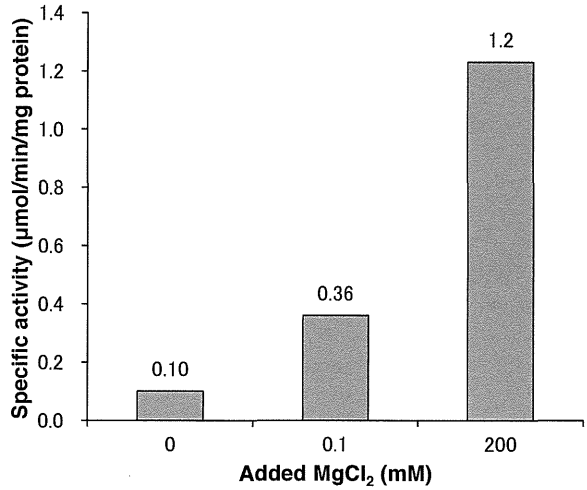

Figure S3 Effect of Mg^{2+} on the specific activity of D-THA DH. EDTA-treated enzyme was prepared using the method described earlier (Maeda et al. 2010). It was incubated for 10 min with the reaction mixture in the absence of any metal, or in the presence of 0.1 or 200 mM $MgCl_2$. The dehydratase activity was then measured. Addition of $MgCl_2$ increases the specific activity of the EDTA-treated D-THA DH.

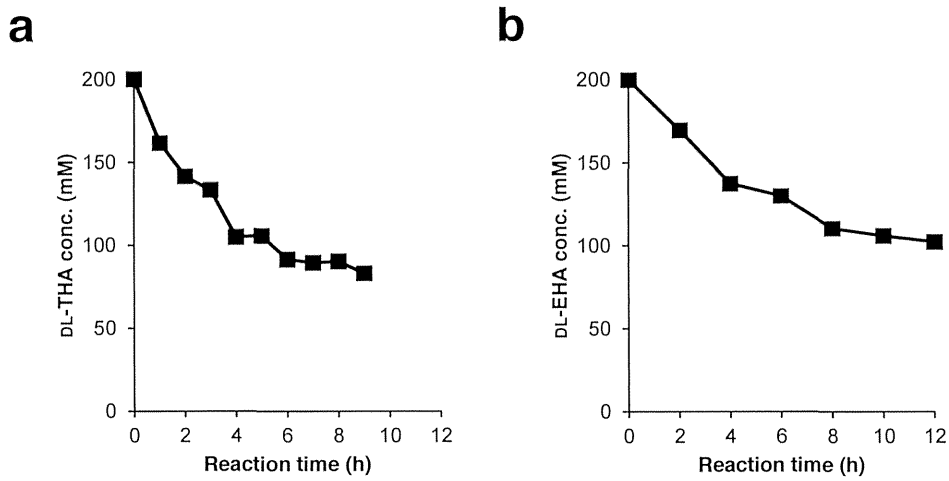

Figure S4 Time-dependent changes in the total concentration of (a) DL-THA and (b) DL-EHA in the reaction mixture. The concentration in the sample of 0 h incubation was taken as 200 mM, and the relative values for following samples were obtained. Total concentration of DL-THA and DL-EHA decreases to about half the initial value when the enantiomeric excess (*e.e.*) of L-THA and D-EHA in the reaction mixture reaches >99%, respectively.

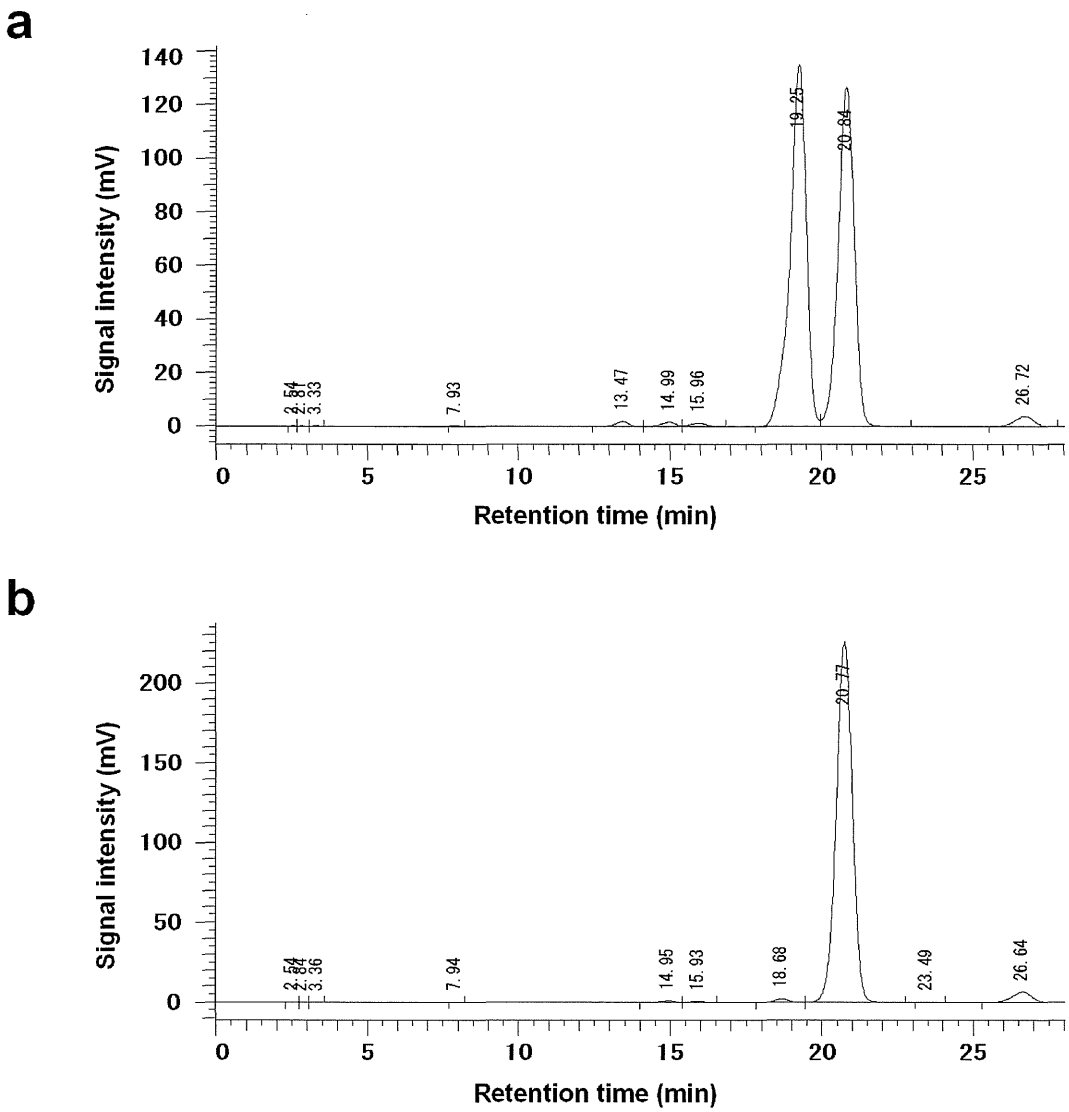

Figure S5 HPLC chromatograms recorded at 250 nm of (a) DL-THA purchased from Tokyo Chemical Industry and (b) L-THA obtained by enzymatic optical resolution. Samples were derivatized with GITC and the derivatives were analyzed using HPLC at a flow rate of 1.0 mL min^{-1} with 30% methanol in water as the mobile phase. Retention times of the D/L-enantiomer of *threo*-3-hydroxyaspartate were 19.25/20.84 min.

a

4185 Matsumoto / L-THA-Enz
Bruker AMX-500/ GC-MS & NMR Lab.
Fac. Agric., Hokkaido Univ.

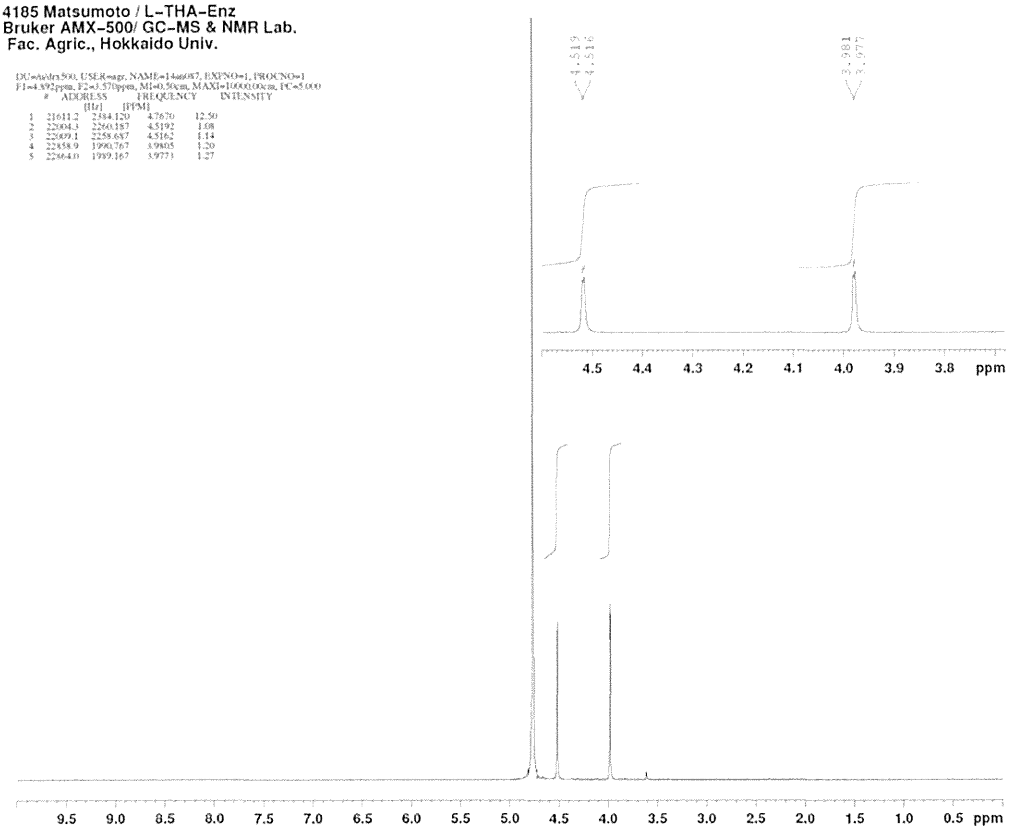

b

4185 Matsumoto / L-THA-Enz
Bruker AMX-500/ GC-MS & NMR Lab.
Fac. Agric., Hokkaido Univ.

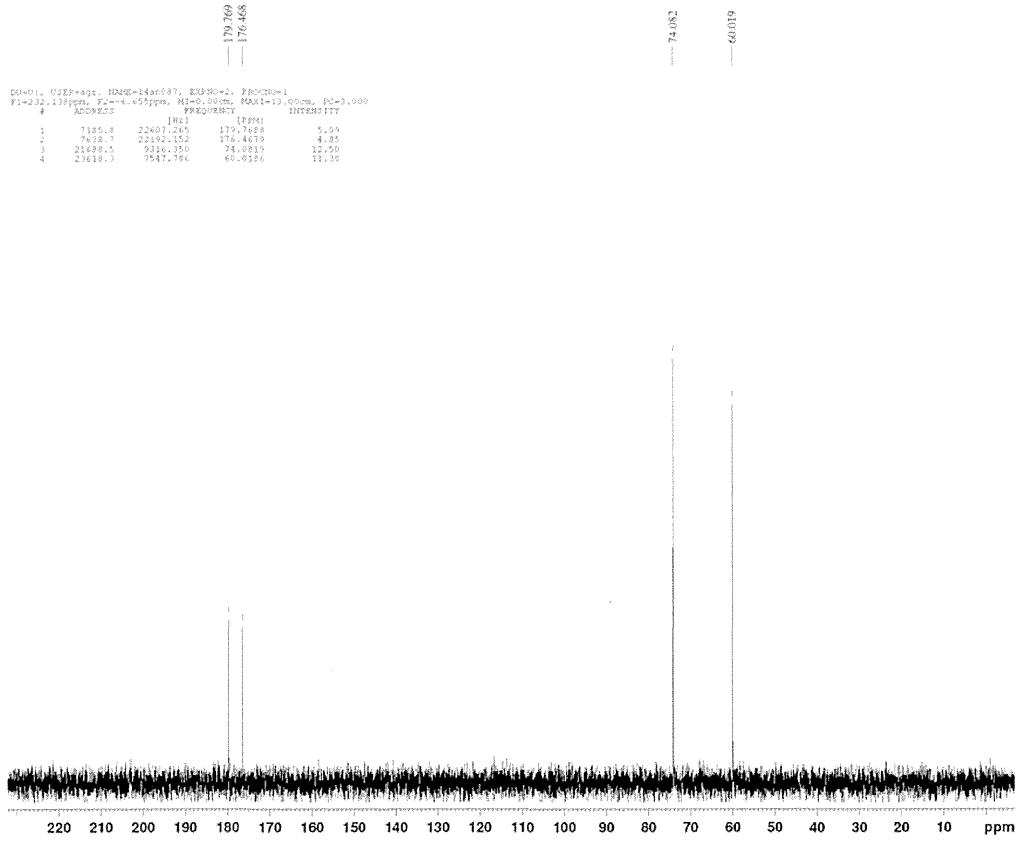

Figure S6 (a) ^{1}H NMR spectra recorded at 500 MHz and (b) ^{13}C NMR spectra recorded at 125 MHz of L-THA obtained by enzymatic optical resolution. Note that the ^{1}H signal at 4.77 ppm is attributed to deuterium oxide (D_2O).

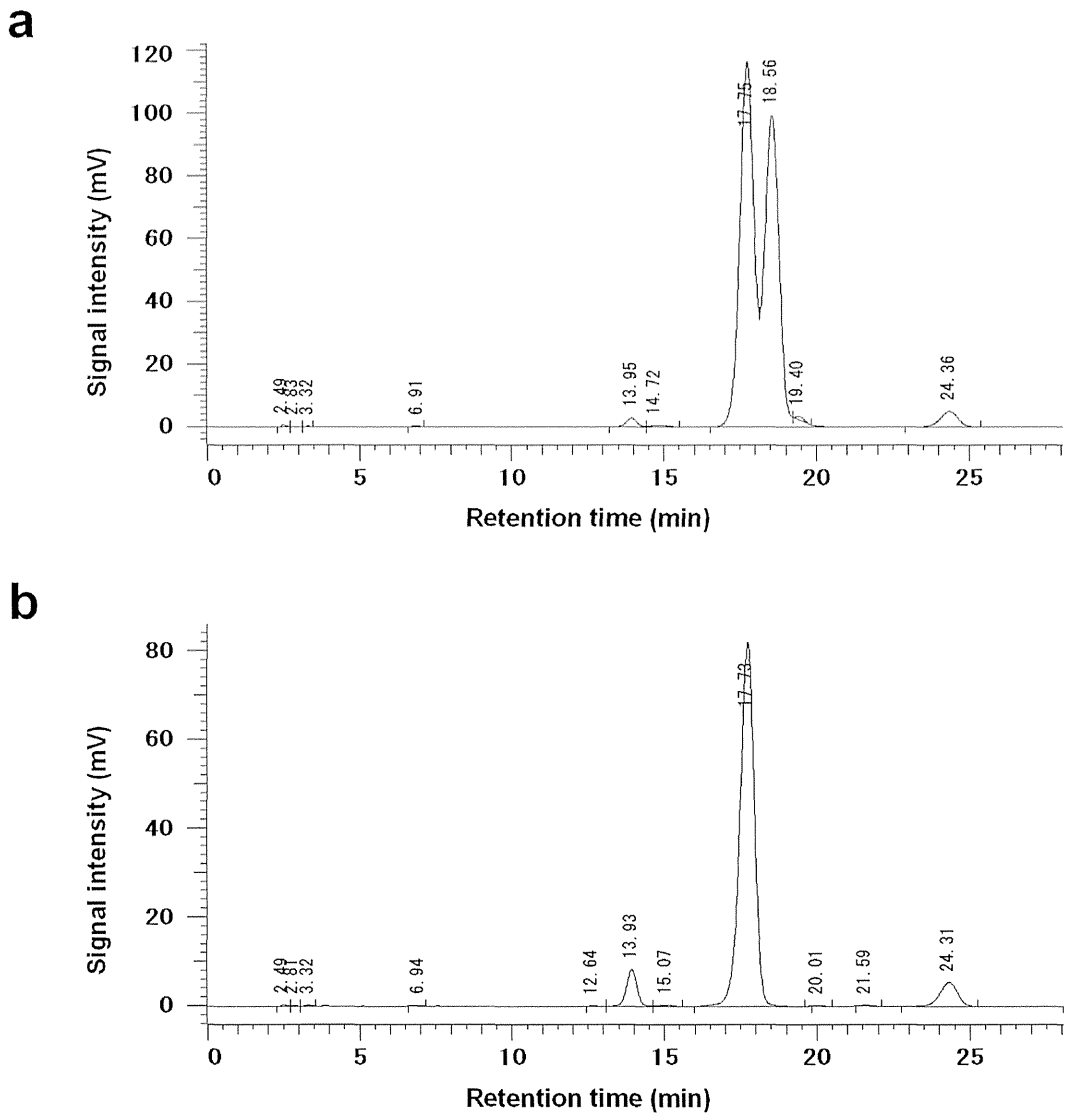

Figure S7 HPLC chromatograms recorded at 250 nm of (a) DL-EHA synthesized by the protocol described in the Materials and methods and (b) D-EHA obtained by enzymatic optical resolution. Samples were derivatized with GITC and the derivatives were analyzed using HPLC at a flow rate of 1.0 mL min^{-1} with 35% methanol in water as the mobile phase. Retention times of the D/L-enantiomer of *erythro*-3-hydroxyaspartate were 17.75/18.56 min.